Hyper-parameters optimized deep feature concatenated network for pediatric pneumonia detection

Mary Shyni Hillary, Chitra Ekambaram

Department of Electronics and Communication Engineering, SRM Institute of Science and Technology, Kattankulathur, India

Article Info

ABSTRACT

Pneumonia, an infection that fills the alveoli of the lung region with pus causes a high rate of chronic illness and fatality amongst children across the globe. The most utilized imaging modality for pediatric pneumonia identification is chest X-rays, whose features are not always readily visible to the naked eye, making it challenging for radiologists to make precise predictions and save lives. Knowing how essential it is to have an early and distinct diagnosis of pneumonia, speeding up or automating the detection process is highly sensible. This article provides a smart, automated system that operates on chest X-ray images and can be successfully utilized for spotting pneumonia. The deep feature concatenation method used by this detection system intends to combine the outcomes of three effective pre-trained models to confirm the reliability of the suggested approach. To obtain its optimal performance, the hyper-parameters are demonstrated using a trial-and-error approach that surpasses existing models with 99.68% accuracy for the early diagnosis of pneumonia. A real-time data sample test is conducted on the proposed pneumonia detection model to evaluate its robustness.

Corresponding Author:

Chitra Ekambaram
Department of Electronics and Communication Engineering, SRM Institute of Science and Technology
Kattankulathur, India
Email: chitrae@srmist.edu.in

1. INTRODUCTION

Pneumonia is a significant threat to children under 5, with an anticipated 11 million deaths by 2030 without intervention. The condition fills alveoli with pus and fluid, making breathing difficult and reducing oxygen intake [1]. Untreated pneumonia can lead to complications like breathing failure and sepsis, even causing death [2]. An individual is bound to get pneumonia as a kid, known as pediatric pneumonia than they are as a grown-up [3].

Pediatric pneumonia, more common in children than adults, exhibits symptoms influenced by the infection's cause, age, and overall health. Common signs include rapid breathing, low oxygen saturation, cough, and high body temperature [4]. Pathogens in a child's nasal passage can harm the lungs when inhaled. Additionally, during and right after childbirth, pneumonia can spread through blood [5].

Chest radiographs are widely used to detect pneumonia, revealing infiltrates as white spots on X-rays [6], [7]. However, examining chest X-rays is difficult and vulnerable to subjectivity [8]. Deep convolutional neural networks (D-CNN) are frequently employed for the analysis of images whose primary function is pattern recognition and as a result, utilized to identify the abnormalities in medical images [9], [10]. Chagas *et al*. [11] employed 12 ImageNet-trained CNNs, enhancing radiographs for infected lung region detection through adaptive histogram equalization. Testing 7 classifiers with pre-trained models, visual geometry group (VGG-19) combined with a support vector machine (SVM) outperformed 84 combinations.

In their study [12], Nalluri and Sasikala proposed a pneumonia screening methodology integrating dynamic histogram equalization (DHE) and median filtering for image enhancement, followed by segmentation using improved watershed segmentation. The researchers devised a method to extract pertinent features and select optimal ones for training deep learning classifiers. Through the utilization of the mean output from these classifiers they achieved a notable detection accuracy of 93.23%.

Fernandes *et al*. [13] introduced a pediatric pneumonia CNN, optimizing hyperparameters through Bayesian optimization. They enhanced VGG-16 with a specialized CNN overlay, achieving optimal F1-score performance despite using pre-processing techniques. According to Mohammed *et al*. [14], the algorithm enhances pneumonia detection using four custom-modified advanced CNN architectures, reducing parameters by exclusively employing convolutional components. It utilizes a SoftMax activation with global average pooling to map to the output layer, generating a heat map for signal strength assessment.

Kermany *et al*. [15] achieved 92.8% accuracy in diagnosing retinal diseases and pediatric pneumonia with Inception V3 transfer learning using 5,232 labeled chest X-ray images subjected to quality control. To overcome the challenge of scarce labeled pneumonia data, Athar employed adversarial training, a method that entails training a secondary network to produce synthetic X-rays resembling real ones but with slight variations. Using a mix of authentic and synthetic X-rays the AlexNet model was trained to achieve an impressive validation accuracy of 98.28% [16].

According to Kundu *et al*. [17], a pneumonia diagnostic system was introduced using weighted ensemble learning, combining three classifiers with weights determined by four assessment criteria and the hyperbolic tangent function. The framework achieved optimal results when all layers were trained on two open-access pneumonia X-ray datasets. Yi *et al*. [18] proposed a deep CNN model with 52 convolutional layers for feature extraction and two dense layers for pneumonia versus normal classification from X-ray and computed tomography (CT) images. The chosen image size of 200×200×3 yielded a precise validation accuracy of 96.09%.

Almaslukh [19] developed a lightweight pneumonia detection model based on DenseNet-121, utilizing random search hyperparameter tuning. Dense connectivity in DenseNet-121 addresses the vanishing gradient issue and promotes feature reuse. The model's reduced parameter count makes it energy-efficient and suitable for rapid detection in medical systems. Alshmrani *et al.* [20] employed the pre-trained VGG 19 network to extract features from chest radiographs, categorizing six distinct lung diseases. To augment the feature extraction capability of VGG 19, the researchers integrated three supplementary convolutional blocks into the network. Following training on 80,000 samples, this adapted network achieved a remarkable testing accuracy of 96.48% [20].

This research optimizes hyper-parameters for a deep feature concatenated model, merging deep features from three successful pre-trained models Inception V3, VGG-16 and DenseNet-201 to mitigate vanishing gradient and overfitting in a binary detection system. The proposed concatenated approach was demonstrated with manual hyper-parameter tuning to obtain an optimal model for precise estimations. Despite the tedious nature of manual tuning, it is valuable for young researchers to grasp hyper-parameter behavior and its impact on network weights.

2.   PROPOSED FINE-TUNED CONCATENATION METHOD

Figure 1 presents the visual layout of the proposed methodology. The framework consists of six main stages: dataset collection and splitting, data pre-processing, transfer learning, model concatenation, hyper-parameter tuning and finally model training and prediction.

2.1. Dataset description

The X-ray images used for the development of the proposed model are from a medical image directory created by Kermany *et al*. [21] which is publicly accessible from the Kaggle database. The directory consists of chest X-ray (CXR) images of children aged from 1 to 5 years provided by the Guangzhou Women and Children's Medical Center. Out of the total 5,856 CXR images, 4,273 are associated with pneumonia, and the remaining 1,583 are healthy. 10% of the normal class has been chosen from each class for testing to prevent class imbalance challenges. Furthermore, ethical approval for the execution of this study was granted by the SRM Medical College Hospital and Research Centre, located in Kattankulathur, India. 13 real-time chest X-ray images including 6 pediatric pneumonia specimens and 4 normal X-rays have been collected which provide diverse set of cases to assess the model's performance across different conditions and scenarios.

2.2. Dataset pre-processing

Normalization in the pre-processing stage speeds up convergence by stabilizing the learning process. In this research, CXR images are scaled from 0-255 to 0-1 by dividing each pixel by 255, ensuring normalization within the range of 0-1 [22]. Data augmentation strategy is implemented to enhance variability

and address class imbalance challenges in the training dataset. Given the substantial number of pneumonia-affected images and a limited number of normal images, potential bias towards the pneumonia class exists [23]. Therefore, for class 0 pneumonia images, augmentation involves clockwise/counterclockwise rotation by 15° and horizontal flipping. To balance data in class 1 (normal images), augmentation includes rotation, horizontal flipping, 20° shear, 20% zoom, 10% left/right shift, and varying brightness from 20 to 90%.
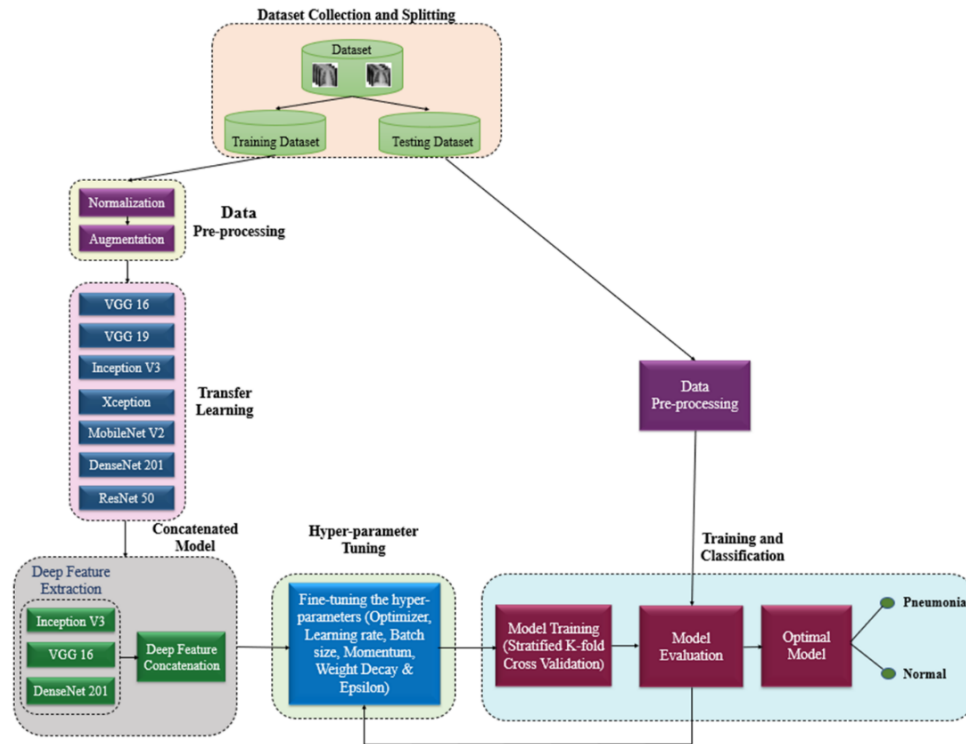

Figure 1. The visual layout of the proposed methodology

2.3. Transfer learning

Transfer learning, the application of knowledge gained from a previous task to enhance learning in a new related task, is employed in this research [24]. Due to limited access to the pediatric pneumonia dataset, seven pre-trained models namely VGG-16, VGG-19, Inception V3, Xception, MobileNet V2, DenseNet-201, and ResNet-50 that are often employed in medical applications and trained with the ImageNet dataset are utilized. The fully connected layer, which served as the final layer in these models alone is retrained without altering the weights of the initial layers.

2.4. Model concatenation

The concatenated model is formed by combining features from the top-performing three out of the seven pre-trained models evaluated on the pediatric pneumonia dataset. The convolutional base of Inception V3, VGG-16, and DenseNet-201 is frozen, serving as feature extractors. Input images propagate forward through these networks, and optimal features are extracted from the layer prior to the fully connected layer [25]. A total of 2,048 features from Inception V3, 512 from VGG-16, and 1,920 from DenseNet-201 are extracted, resulting in a concatenated model with 4,480 features. These feature sets are then fed into a reshaped fully connected layer, followed by a sigmoid classifier for pneumonia and normal CXR image classification.

2.5. Hyper-parameter tuning

Hyper-parameter tuning is an imperative perspective that outcomes in the best execution of the model by tracking the right combination of hyper-parameters in a sensible measure of time [26]. For a more reliable and optimized model, optimal hyper-parameters must be defined prior to data fitting because they vary for distinct datasets [27]. The hyperparameters are demonstrated using a trial-and-error approach to obtain the optimal performance of the proposed concatenated model, and the optimal model is utilized to detect pneumonia in children.

The preliminary step is to select the optimizer, which is an algorithm used to update the various attributes of the model to minimize the losses. The Adam optimizer performed well with our dataset. Upon selection of the optimizer, the model is validated for optimum performance using a range of learning rates and batch sizes. After the learning rate and batch size are set to the desired levels the model is evaluated with different values of momentum to achieve its optimal value. The model is assessed for various weight decay and epsilon values to determine its ideal value. Finally, a learning rate adjustment has been made which produced meaningful improvements.

2.6. Model training and prediction

The concatenated model is trained and validated for 50 epochs using 10-fold cross-validation, reducing bias and improving generalization. The training involved randomly dividing the dataset into 10 folds (9:1 split for training and validation) across ten iterations [28]. The average accuracy obtained in each iteration is the final accuracy of the model.

Starting with randomly initialized weights and biases, the model's predicted outputs are compared with actual outputs. Weights and biases are then updated and backpropagated through initial layers based on the loss function, aiming to minimize loss and improve accuracy [29]. Training continued until parameter updates no longer enhanced validation accuracy, employing early stopping with a patience value of 5. Classification utilized the fully connected layer with a sigmoid activation function for binary output corresponding to pneumonia and normal cases.

3.   RESULTS AND DISCUSSION

The proposed concatenated model is refined systematically to enhance its effectiveness in detecting pediatric pneumonia from chest radiographs. The fine-tuning process begins with pre-training on a diverse dataset, allowing the model to learn fundamental patterns and features relevant to medical imaging. Subsequently, the model undergoes iterative adjustments, including domain-specific training, hyperparameter optimization, and performance evaluation, to ensure it achieves high accuracy and reliability in pneumonia classification.

3.1. Performance metrics

Performance metrics evaluate the performance of the deep learning model based on its ability to forecast unobserved data. The predicted outcomes of the models are visualized in the form of a confusion matrix that has 4 entries: i) true positives (TP): correctly predicted pneumonia cases, ii) true negatives (TN): correctly predicted normal cases, iii) false positives (FP): incorrectly predicted normal cases, and iv) false negatives (FN): incorrectly predicted pneumonia cases [30]. Table 1 displays the metrics used to evaluate the performance of the proposed model.

Table 1. Metrics used to evaluate the performance of the model

Metrics	Formula
Accuracy	$\dfrac{TP + TN}{TN + TP + FN + FP}$
Precision	$\dfrac{TP}{TP + FP}$
Recall	$\dfrac{TP}{TP + FN}$
F1-score	$2 \times \dfrac{Precision \times Recall}{Precision + Recall}$
Specificity	$\dfrac{TN}{TN + FP}$
MCC	$\dfrac{TN \times TP - FN \times FP}{\sqrt{(TP + FP)(TP + FN)(TN + FP)(TN + FN)}}$

3.2. Results

The concatenation method in this detection system integrates features from three pre-trained models: Inception V3, VGG-16, and DenseNet-201, chosen based on their performance metrics among seven evaluated models widely used in medical diagnostics. Evaluation metrics in Table 2 indicate that VGG-16 and Inception V3 achieved the highest accuracy score of 94.94%. Considering other metrics like precision, specificity, and Matthew correlation coefficient (MCC), Inception V3 outperformed VGG-16 with 100% precision and specificity. Similarly, DenseNet-201 outperformed VGG-19 with an accuracy of 93.67%, demonstrating 100% precision and specificity. Figures 2(a) to 2(c) depicts the confusion matrix for the three best-performed models on the test data.

Table 2. Classification results of the seven pre-trained models

| Model | TP | TN | FP | FN | Performance (%) | | | | | MCC |
					Accuracy	Precision	Sensitivity	F1-score	Specificity	
VGG-16	143	157	1	15	94.94	99.31	90.51	94.70	99.37	0.9023
VGG-19	139	157	1	19	93.67	99.29	87.97	93.29	99.37	0.8791
Inception V3	142	158	0	16	94.94	100	89.87	94.67	100	0.9034
Xception	134	156	2	24	91.77	98.53	84.81	91.16	98.73	0.8437
MobileNet V2	136	156	2	22	92.41	98.55	86.08	91.89	98.73	0.8549
DenseNet-201	138	158	0	20	93.67	100	87.34	93.24	100	0.8805
ResNet-50	123	157	1	35	88.61	99.19	77.85	87.23	99.37	0.7907
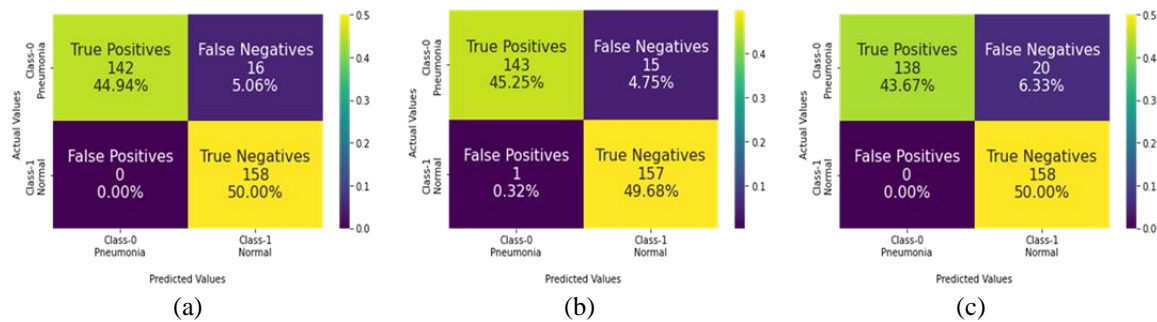
Figure 2. Confusion matrix for the three best-performed models of (a) Inception V3, (b) VGG-16, and (c) DenseNet-201

The best features of the top 3 models Inception V3, VGG-16, and DenseNet-201 are combined to develop the concatenated model. Table 3 highlights the performance of the concatenated model. In comparison to the individual performances of the three models, the concatenated model performs better. The concatenated model achieved an accuracy of 98.73% which is almost a 4% increase when compared with the individual performance. The accuracy of the concatenated model increased as a result of a sharp increase in the true positive value. The true positive value for the concatenated model is 155, which indicates that out of the 158 pneumonia cases 155 are correctly classified as pneumonia and 3 are misclassified as normal. The true negative value is 157, which indicates that out of the 158 normal cases, 157 are correctly classified as normal while 1 instance is misclassified as pneumonia.

Table 3. Performance metrics of the concatenated model

| Model | TP | TN | FP | FN | Performance (%) | | | | | MCC |
					Accuracy	Precision	Sensitivity	F1 score	Specificity	
Inception V3	142	158	0	16	94.94	100	89.87	94.67	100	0.9034
VGG-16	143	157	1	15	94.94	99.31	90.51	94.70	99.37	0.9023
DenseNet-201	138	158	0	20	93.67	100	87.34	93.24	100	0.8805
Concatenated model	155	157	1	3	98.73	99.36	98.10	98.73	99.37	0.9748

3.2.1. Optimizer selection

The concatenated model, developed by merging features from three models, is trained using the Adam optimizer. To identify the most effective optimization approach, the model is also assessed with alternative algorithms, including RMSProp, stochastic gradient descent (SGD), Adadelta, and Adagrad. Results in Table 4 reveal that the model excels with Adam optimization compared to other algorithms. Throughout the entire fine-tuning process, the Adam optimization algorithm consistently maintained a high accuracy of 98.73% with the pediatric pneumonia dataset.

3.2.2. Optimal learning rate selection

The model is initially trained with the Adam optimizer's default learning rate of 0.001. Experimentation with different learning rates, including 1e-2, 1e-4, and 1e-5, is conducted. Table 4 presents the classification results, indicating improved accuracy at a learning rate of 1e-4. Consequently, the learning rate is fixed at 1e-4 for further model tuning. The concatenated model achieved an accuracy of 99.05%, correctly classifying 156 pneumonia cases and 157 normal cases, with only 2 and 1 misclassifications, respectively.

Table 4. Hyper-parameter optimization of the concatenated model

Hyper-parameters		TP	TN	FP	FN	Performance (%)					MCC
						Accuracy	Precision	Sensitivity	F1 score	Specificity	
Optimization algorithm	Adam	155	157	1	3	98.73	99.36	98.10	98.73	99.37	0.9748
	RMSProp	152	158	0	6	98.10	100	96.20	98.06	100	0.9627
	SGD	153	157	1	5	98.10	99.35	96.84	98.08	99.37	0.9627
	Adadelta	142	158	0	16	94.94	100	89.87	94.67	100	0.9034
	Adagrad	136	156	2	22	92.41	98.55	86.08	91.89	98.73	0.8549
Learning rate	0.01	152	158	0	6	98.10	100	96.20	98.06	100	0.9627
	0.001	155	157	1	3	98.73	99.36	98.10	98.73	99.37	0.9748
	1e-4	156	157	1	2	99.05	99.36	98.73	99.05	99.37	0.9810
	1e-5	152	158	0	6	98.10	100	96.20	98.06	100	0.9627
Batch size	16	152	158	0	6	98.10	100	96.20	98.06	100	0.9627
	25	153	158	0	5	98.42	100	96.84	98.39	100	0.9688
	30	151	158	0	7	97.78	100	95.57	97.73	100	0.9566
	32	156	157	1	2	99.05	99.36	98.73	99.05	99.37	0.9810
	35	153	158	0	5	98.42	100	96.84	98.39	100	0.9688
	40	151	158	0	7	97.78	100	95.57	97.73	100	0.9566
	64	151	158	0	7	97.78	100	95.57	97.73	100	0.9566
Momentum	β_1=0.9 β_2=0.999	156	157	1	2	99.05	99.36	98.73	99.05	99.37	0.9810
	β_1=0.92 β_2=0.999	151	158	0	7	97.78	100	95.57	97.73	100	0.9566
	β_1=0.95 β_2=0.999	152	158	0	6	98.10	100	96.20	98.06	100	0.9627
	β_1=0.99 β_2=0.999	153	158	0	5	98.42	100	96.84	98.39	100	0.9688
	β_1=0.992 β_2=0.999	153	158	0	5	98.42	100	96.84	98.39	100	0.9688
	β_1=0.999 β_2=0.999	151	158	0	7	97.78	100	95.57	97.73	100	0.9566
	β_1=0.88 β_2=0.999	151	158	0	7	97.78	100	95.57	97.73	100	0.9566
	β_1=0.8 β_2=0.999	153	158	0	5	98.42	100	96.84	98.39	100	0.9688
	β_1=0.7 β_2=0.999	153	158	0	5	98.42	100	96.84	98.39	100	0.9688
	β_1=0.9 β_2=0.997	154	158	0	4	98.73	100	97.47	98.72	100	0.9750
	β_1=0.9 β_2=0.99	156	158	0	2	99.37	100	98.73	99.36	100	0.9874
	β_1=0.9 β_2=0.992	153	158	0	5	98.42	100	96.84	98.39	100	0.9688
	β_1=0.9 β_2=0.97	154	158	0	4	98.73	100	97.47	98.72	100	0.9750
	β_1=0.9 β_2=0.9	154	157	1	4	98.42	99.35	97.47	98.40	99.37	0.9685
	β_1=0.9 β_2=0.92	152	158	0	6	98.10	100	96.20	98.06	100	0.9627
Weight decay	0	156	158	0	2	99.37	100	98.73	99.36	100	0.9874
	0.1	132	158	0	26	91.77	100	83.54	91.03	100	0.8470
	1e-2	147	158	0	11	96.52	100	93.04	96.39	100	0.9326
	1e-3	152	158	0	6	98.10	100	96.20	98.06	100	0.9627
	1e-4	152	158	0	6	98.10	100	96.20	98.06	100	0.9627
	1e-5	151	158	0	7	97.78	100	95.57	97.73	100	0.9566
	1e-6	151	158	0	7	97.78	100	95.57	97.73	100	0.9566
Epsilon	1e-7	156	158	0	2	99.37	100	98.73	99.36	100	0.9874
	1e-8	152	157	1	6	97.78	99.35	96.20	97.75	99.37	0.9562
	1e-6	151	158	0	7	97.78	100	95.57	97.73	100	0.9566
	1e-3	151	158	0	7	97.78	100	95.57	97.73	100	0.9566
	0.1	151	158	0	7	97.78	100	95.57	97.73	100	0.9566
	1	147	158	0	11	96.52	100	93.04	96.39	100	0.9326

3.2.3. Optimal batch size selection

The model which is already trained with batch size 32 underwent additional training with a range of batch sizes to obtain the optimal value. The outcomes in Table 4 demonstrate how the model performs with various batch sizes. It can be seen from the table that higher performance is obtained with a batch size of 32. The model is further adjusted for other hyper-parameters after fixing the batch size to 32.

3.2.4. Optimal momentum selection

The concatenated model, initially trained with the default momentum values of the Adam optimizer β1=0.9 and β2=0.999, is further evaluated with various momentum values. Table 4 displays the model's performance, indicating that the combination of β1=0.9 and β2=0.99 achieved the highest accuracy at 99.37%. With 100% precision and specificity, all normal cases are correctly classified, while 2 out of 158 pneumonia cases are misclassified as normal. These momentum values β1=0.9 and β2=0.99 are then frozen before proceeding to the next tuning stages.

3.2.5. Optimal weight decay selection

The model which is initially trained with the default weight decay of 0 is further trained with different values to get the optimal one. The classification results of the concatenated model with different values of weight decay are shown in Table 4. However, the performance of the model has shown no improvement with values greater than 0 and therefore we have considered using the default weight decay.

3.2.6. Optimal epsilon selection

The model is trained with different values of epsilon whose performance is presented in Table 4. The model has shown better performance with the default epsilon value 1e-7 in comparison with other values. Hence the default epsilon value has been chosen for the model.

3.2.7. Fine-tuning the learning rate

After tuning all hyper-parameters, the final adjustment of the learning rate significantly improved the model's accuracy to 99.68%. With a learning rate of 2e-4 (0.0002), the model correctly classifies all normal cases and misclassifies only one pneumonia case as shown in Table 5. The optimal hyper-parameters obtained are: learning rate=2e-4, batch size=32, momentum: $\beta 1=0.9$ and $\beta 2=0.99$, weight decay=0, and epsilon=1e-7. The confusion matrix and receiver operating characteristic (ROC) curve of the proposed model are presented in Figures 3(a) and 3(b).

Table 5. Performance of the concatenated model with fine-tuned learning rate

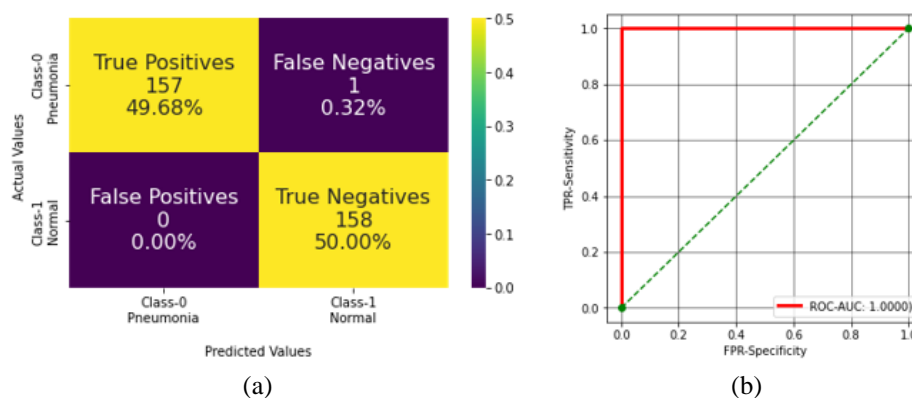| Learning rate	TP	TN	FP	FN	Performance (%)					MCC
					Accuracy	Precision	Sensitivity	F1 score	Specificity	
1e-4	156	158	0	2	99.37	100	98.73	99.36	100	0.9874
0.008	156	157	1	2	99.05	99.36	98.73	99.05	99.37	0.9810
0.005	152	158	0	6	98.10	100	96.20	98.06	100	0.9627
2e-4	157	158	0	1	99.68	100	99.37	99.68	100	0.9937
3e-4	152	158	0	6	98.10	100	96.20	98.06	100	0.9627

(a)   (b)

Figure 3. Confusion matrix and ROC curve of the proposed model of (a) confusion matrix and (b) ROC curve

3.3. Real-time testing

13 real-time samples obtained from SRM Medical College Hospital and Research Centre are used to assess the robustness of the model. The database includes 6 pediatric pneumonia specimens and 4 normal X-rays. The model accurately categorizes every sample, yielding a 100% accuracy rate.

4. CONCLUSION

Pneumonia causes pleural effusion that leads to a fatality rate of 15% in children below the age of 5. An early diagnosis of the disease and prompt medical intervention can limit the ramifications and potentially save the lives of thousands of children. The contribution of this research is the proposal of a diagnostic framework for pediatric pneumonia based on concatenation and optimization. The concatenation methodology employed in this detection system integrates the performance of three successful pre-trained models Inception V3, VGG-16 and DenseNet-201. The aim is to enhance the accuracy of the concatenated model by optimizing the hyper-parameters to provide more precise estimates. A step-by-step optimization is carried out with the Adam optimizer and the following optimal hyper-parameters are obtained: learning rate=2e-4, batch size=32, momentum: $\beta 1=0.9$ and $\beta 2=0.99$, weight decay=0 and epsilon=1e-7. The proposed fine-tuned concatenated model outperformed other existing models with an accuracy of 99.68%. We have reached an important conclusion that hyper-parameter optimization is an essential procedure to obtain the best results from the

model. However, the suggested model entails considerable computational expenses due to the concatenation and manual optimization methods employed. In the future, we would extend our research to develop an optimal model for multiclass lung disease classification.

FUNDING INFORMATION
The authors declare that no funding was received for conducting this research.

AUTHOR CONTRIBUTIONS STATEMENT
This journal uses the Contributor Roles Taxonomy (CRediT) to recognize individual author contributions, reduce authorship disputes, and facilitate collaboration.

Name of Author	C	M	So	Va	Fo	I	R	D	O	E	Vi	Su	P	Fu
Mary Shyni Hillary	✓	✓	✓				✓		✓					
Chitra Ekambaram				✓	✓	✓		✓		✓	✓	✓		

C : **C**onceptualization	I : **I**nvestigation	Vi : **Vi**sualization
M : **M**ethodology	R : **R**esources	Su : **Su**pervision
So : **So**ftware	D : **D**ata Curation	P : **P**roject administration
Va : **Va**lidation	O : Writing - **O**riginal Draft	Fu : **Fu**nding acquisition
Fo : **Fo**rmal analysis	E : Writing - Review & **E**diting	

CONFLICT OF INTEREST STATEMENT
Authors state no conflict of interest.

INFORMED CONSENT
We have obtained informed consent from all individuals included in this study.

DATA AVAILABILITY
Data availability is not applicable to this paper as no new data were created or analyzed in this study.

REFERENCES
[1]   C. J. Abeja, V. Niyonzima, J. P. Byagamy, and C. Obua, "Antibiotic prescription rationality and associated in-patient treatment outcomes in children under-five with severe pneumonia at Bwizibwera Health Center IV, Mbarara District, South-Western Uganda," *Pneumonia*, vol. 14, no. 1, 2022, doi: 10.1186/s41479-022-00095-0.
[2]   G. Labhane, R. Pansare, S. Maheshwari, R. Tiwari, and A. Shukla, "Detection of pediatric pneumonia from chest X-ray images using CNN and transfer learning," *2020 3rd International Conference on Emerging Technologies in Computer Engineering: Machine Learning and Internet of Things (ICETCE)*, Jaipur, India, 2020, pp. 85-92, doi: 10.1109/ICETCE48199.2020.9091755.
[3]   E. T. Salah, S. H. Algasim, A. S. Mhamoud, and N. E. O. S. A. Husian, "Prevalence of hypoxemia in under-five children with pneumonia in an emergency pediatrics hospital in Sudan," *Indian Journal of Critical Care Medicine*, vol. 19, no. 4, pp. 203–207, 2015, doi: 10.4103/0972-5229.154549.
[4]   D. K. Smith, D. P. Kuckel, and A. M. Recidoro, "Community-acquired pneumonia in children: rapid evidence review," *American Family Physician*, vol. 104, no. 6, pp. 618-625, 2021.
[5]   P. Dean and T. A. Florin, "Factors associated with pneumonia severity in children: a systematic review," *Journal of the Pediatric Infectious Diseases Society*, vol. 7, no. 4, pp. 323–334, 2018, doi: 10.1093/jpids/piy046.
[6]   T. P. Htun, Y. Sun, H. L. Chua, and J. Pang, "Clinical features for diagnosis of pneumonia among adults in primary care setting: A systematic and meta-review," *Scientific Reports*, vol. 9, no. 1, 2019, doi: 10.1038/s41598-019-44145-y.
[7]   S. Singh, "Efficient pneumonia detection using vision transformers on chest X-rays," *Scientific Reports*, vol. 14, 2024, doi: 10.1038/s41598-024-52703-2.
[8]   M. Mujahid, F. Rustam, R. Álvarez, J. L. V. Mazón, I. de la T. Díez, and I. Ashraf, "Pneumonia classification from X-ray images with Inception-V3 and convolutional neural network," *Diagnostics*, vol. 12, no. 5, 2022, doi: 10.3390/diagnostics12051280.
[9]   E. Çallı, E. Sogancioglu, B. V. Ginneken, K. G. V. Leeuwen, and K. Murphy, "Deep learning for chest X-ray analysis: A survey," *Medical Image Analysis*, vol. 72, 2021, doi: 10.1016/j.media.2021.102125.
[10]   S. Iqbal, A. N. Qureshi, J. Li, and T. Mahmood, "On the analyses of medical images using traditional machine learning techniques and convolutional neural networks," *Archives of Computational Methods in Engineering*, vol. 30, no. 5, pp. 3173–3233, 2023, doi: 10.1007/s11831-023-09899-9.
[11]   J. V. S. D. Chagas, D. D. A Rodrigues, R. F. Ivo, M. M. Hassan, V. H. C. de Albuquerque, and P. P. R. Filho, "A new approach for the detection of pneumonia in children using CXR images based on an real-time IoT system," *Journal of Real-Time Image Processing*, vol. 18, no. 4, pp. 1099–1114, 2021, doi: 10.1007/s11554-021-01086-y.
[12]   S. Nalluri and R. Sasikala, "Pneumonia screening on chest X-rays with optimized ensemble model," *Expert Systems with Applications*, vol. 242, 2024, doi: 10.1016/j.eswa.2023.122705.

[13] V. Fernandes, G. B. Junior, A. C. de Paiva, A. C. Silva, and M. Gattass, "Bayesian convolutional neural network estimation for pediatric pneumonia detection and diagnosis," *Computer Methods and Programs in Biomedicine*, vol. 208, 2021, doi: 10.1016/j.cmpb.2021.106259.

[14] I. Mohammed, N. Singh, and M. Venkatasubramanian, *Computer-assisted detection and diagnosis of pediatric pneumonia in chest x-ray images*, Friday Harbor, USA: Pattern Computer 2019.

[15] D. S. Kermany *et al.*, "Identifying medical diagnoses and treatable diseases by image-based deep learning," *Cell*, vol. 172, no. 5, pp. 1122-1131, 2018, doi: 10.1016/j.cell.2018.02.010.

[16] A. Athar, "Improving pneumonia detection in chest x-rays using transfer learning approach (AlexNet) and adversarial training," *2023 International Conference on Business Analytics for Technology and Security (ICBATS)*, Dubai, United Arab Emirates, 2023, pp. 1-7, doi: 10.1109/ICBATS57792.2023.10111193.

[17] R. Kundu, R. Das, Z. W. Geem, G.-T. Han, and R. Sarkar, "Pneumonia detection in chest X-ray images using an ensemble of deep learning models," *PLoS One*, vol. 16, no. 9, 2021, doi: 10.1371/journal.pone.0256630.

[18] R. Yi, L. Tang, Y. Tian, J. Liu, and Z. Wu, "Identification and classification of pneumonia disease using a deep learning-based intelligent computational framework," *Neural Computing and Applications*, vol. 35, no. 20, 2023, doi: 10.1007/s00521-021-06102-7.

[19] B. Almaslukh, "A lightweight deep learning-based pneumonia detection approach for energy-efficient medical systems," *Wireless Communications and Mobile Computing*, vol. 2021, no. 1. 2021, doi: 10.1155/2021/5556635.

[20] G. M. M. Alshmrani, Q. Ni, R. Jiang, H. Pervaiz, and N. M. Elshennawy, "A deep learning architecture for multi-class lung diseases classification using chest X-ray (CXR) images," *Alexandria Engineering Journal*, vol. 64, 2023, doi: 10.1016/j.aej.2022.10.053.

[21] D. Kermany, K. Zhang, and M. Goldbaum, "Labeled optical coherence tomography (OCT) and chest x-ray images for classification," *Mendeley data*, 2018, doi: 10.17632/rscbjbr9sj.2.

[22] S. R. Nayak, D. R. Nayak, U. Sinha, V. Arora, and R. B. Pachori, "Application of deep learning techniques for detection of COVID-19 cases using chest X-ray images: a comprehensive study," *Biomedical Signal Processing and Control*, vol. 64, 2021, doi: 10.1016/j.bspc.2020.102365.

[23] M. M. Rahman and D. N. Davis, "Addressing the class imbalance problem in medical datasets," *International Journal of Machine Learning and Computing*, vol. 32, no. 2, pp. 224–228, 2013.

[24] F. Zhuang *et al.*, "A comprehensive survey on transfer learning," *Proceedings of the IEEE,* vol. 109, no. 1, pp. 43-76, Jan. 2021, doi: 10.1109/JPROC.2020.3004555.

[25] M. Rahimzadeh and A. Attar, "A modified deep convolutional neural network for detecting COVID-19 and pneumonia from chest X-ray images based on the concatenation of Xception and ResNet50V2," *Informatics in Medicine Unlocked*, vol. 19, 2020, doi: 10.1016/j.imu.2020.100360.

[26] A. Morales-Hernández, I. V. Nieuwenhuyse, and S. R. Gonzalez, "A survey on multi-objective hyperparameter optimization algorithms for machine learning," *Artificial Intelligence Review*, vol. 56, no. 8, pp. 8043–8093, 2023, doi: 10.1007/s10462-022-10359-2.

[27] S. Y. Sen and N. Ozkurt, "Convolutional neural network hyperparameter tuning with Adam optimizer for ECG classification," *2020 Innovations in Intelligent Systems and Applications Conference (ASYU)*, 2020, pp. 1-6, doi: 10.1109/ASYU50717.2020.9259896.

[28] S. Yadav and S. Shukla, "Analysis of k-fold cross-validation over hold-out validation on colossal datasets for quality classification," in *2016 IEEE 6th International Conference on Advanced Computing (IACC),* 2016, pp. 78-83, doi: 10.1109/IACC.2016.25.

[29] M. C. Arellano and O. E. Ramos, "Deep learning model to identify COVID-19 cases from chest radiographs," *2020 IEEE XXVII International Conference on Electronics, Electrical Engineering and Computing (INTERCON)*, Lima, Peru, 2020, pp. 1-4, doi: 10.1109/INTERCON50315.2020.9220237.

[30] D. Chicco and G. Jurman, "A statistical comparison between Matthews correlation coefficient (MCC), prevalence threshold, and Fowlkes-Mallows index," *Journal of Biomedical Informatics*, vol. 144, 2023, doi: 10.1016/j.jbi.2023.104426.

BIOGRAPHIES OF AUTHORS

Mary Shyni Hillary [ID] [GS] [SC] [pub] received her B.E. in electronics and communication engineering from DMI College of Engineering, Chennai, India and her M.Tech. degree in laser and electro-optical engineering from College of Engineering Guindy, Anna University, Chennai, India. She is pursuing her Ph.D. as a full-time research scholar in the Department of Electronics and Communication Engineering at SRM Institute of Science and Technology, Kattankulathur, Tamil Nadu, India. She has 6 years of academic teaching experience. Her research area includes image processing, machine learning, and deep learning. She can be contacted at email: mh3006@srmist.edu.in.

Dr. Chitra Ekambaram [ID] [GS] [SC] [pub] is an Assistant Professor in the Department of Electronics and Communication Engineering at SRM Institute of Science & Technology, Kattankulathur, Tamil Nadu, India since 2006. She obtained her Ph.D. degree from SRM Institute of Science & Technology, Kattankulathur. She has 22 years of experience in managing undergraduate, and postgraduate programs and supervising research projects. Her research interests include VLSI low power high-speed design, DSP structures and VLSI design automation, image processing, machine learning, and deep learning. She can be contacted at email: chitrae@srmist.edu.in.